Rock and Soil Mechanics

Volume 42 | Issue 7 Article 7

11-23-2021

# Effects of cyclic loading directions on liquefaction characteristics of saturated coral sand

Kang LIU
*Institute of Geotechnical Engineering, Nanjing Tech. University, Nanjing, Jiangsu 210009, China*

Guo-xing CHEN
*Civil Engineering and Earthquake Disaster Prevention Center of Jiangsu Province, Nanjing, Jiangsu 210009, China*, gxc6307@163.com

Qi WU
*Civil Engineering and Earthquake Disaster Prevention Center of Jiangsu Province, Nanjing, Jiangsu 210009, China*

Wei-jia MA
*Institute of Geotechnical Engineering, Nanjing Tech. University, Nanjing, Jiangsu 210009, China*

*See next page for additional authors*



## Custom Citation

LIU Kang, CHEN Guo-xing, WU Qi, MA Wei-jia, QIN You, . Effects of cyclic loading directions on liquefaction characteristics of saturated coral sand[J]. Rock and Soil Mechanics, 2021, 42(7): 1951-1960.

# Effects of cyclic loading directions on liquefaction characteristics of saturated coral sand


## Authors

Kang LIU, Guo-xing CHEN, Qi WU, Wei-jia MA, and You QIN

Rock and Soil Mechanics 2021 42(7): 1951−1960 ISSN 1000−7598
https: //doi.org/10.16285/j.rsm.2020.6728 rocksoilmech.researchcommons.org/journal

# Effects of cyclic loading directions on liquefaction characteristics of saturated coral sand

LIU Kang[1], CHEN Guo-xing[1, 2], WU Qi[1, 2], MA Wei-jia[1], QIN You[1]

1. Institute of Geotechnical Engineering, Nanjing Tech. University, Nanjing, Jiangsu 210009, China
2. Civil Engineering and Earthquake Disaster Prevention Center of Jiangsu Province, Nanjing, Jiangsu 210009, China

**Abstract:** The large scale construction of both military and civil infrastructures located in Nansha reefs and offshore marine areas, South China Sea, has raised the seismic safety a challenging issue for the projects in the region. The influences of fines content (FC) on the liquefaction characteristics of saturated terrestrial quartz sands have been extensively studied, but the corresponding research on saturated coral sands in reclaimed coral islands is less involved. Using the GDS hollow cylinder torsion shear apparatus, a series of isotropically consolidated undrained cyclic tests have been performed on saturated coral sand sampled from the Nansha Islands, South China Sea. The samples are prescribed with the stress path formed under the 90° jump rotation of principal stress with various cyclic loading directions. The influences of the inclination angle ($\alpha_d$) of the major principal stress and fines content FC on the liquefaction characteristics of saturated coral sand are investigated. It has been discovered that, regarding the zero effective stress state as initial liquefaction criterion, the liquefaction resistance of saturated coral sand decreases with the increase of $\alpha_d$ for $0°\leqslant\alpha_d\leqslant45°$ and FC for $0\%\leqslant FC\leqslant30\%$. The correlation among the generalized shear strain amplitude ($\gamma_{ga}$), the fines content FC, and the revolution of residual excess pore water pressure of saturated coral soil has been clearified. By introducing a unit cyclic stress ratio USR as a new index for liquefaction resistance and based on binary medium theory, the expression between the unit cyclic stress ratio $USR_{15}$, inducing initial liquefaction in 15 cycles, and the equivalent skeleton void ratio $e_{sk}^{*}$ for the saturated sands is established for the test. The theory is validated by the experimental data in the literature.

**Keyword:** saturated coral sand; cyclic loading direction; fines content; excess pore water pressure; liquefaction resistance

## 1 Introduction

Calcareous sand is defined as the carbonate sediments with high calcium carbonate ($CaCO_3$) content mainly composed of calcite and aragonite. Tropical and subtropical coral reefs are the main source of calcareous sand with $CaCO_3$ content greater than 90%, and this material is usually called coral sand. The undrained behavior of coral sand under cyclic loading caused by earthquake and ocean wave is an important topic in geotechnical engineering field. The earthquake causes severe geotechnical disasters of coral sand sediments, shown in the 1993 Guam earthquake[1], the 2006 Hawaii earthquake[2] and the 2010 Haiti earthquake[3]. As recorded in the literature[4], a lot of strong earthquakes and destructive earthquakes have occurred in the Nansha Islands area in the last one hundred years, and therefore, this geotechnic hazard would be challenging for coral reef projects.

The undrained dynamic characteristics of saturated sand under complex stress conditions caused by seismic P-S wave coupling, especially the liquefaction phenomenon, is a long-term concern but unsolved problem. Guo et al.[5] found that the pattern of principal stress direction has little effect on the relationship between pore pressure ratio and generalized shear strain of Fujian standard sand. However, when the principal stress axis rotates continuously, the lowest liquefaction strength CRR of saturated sand is obtained. The test results of Li[6] and Yu[7] show that the lowest strength CRR of calcareous sand occurs under the circular stress path. Xu et al.[8] found that the phase difference and amplitude ratio of axial and torsional shear dynamic loads have a significant impact on the development of excess pore water pressure and CRR of saturated sand. Huang et al.[9] studied the influence of cyclic loading stress path on the deformation development mode of loose Fujian standard sand and dense Qiantang River silt, and used the equivalent cyclic stress ratio ESR to characterize the standardized CRR curve under cyclic loading of different oblique elliptical stress paths. Sivathayalan et al.[10] conducted a series of uniformly consolidated undrained cyclic shear tests on loose sand. The results show that the

Received: 20 November 2020 Revised: 20 April 2021
This work was supported by the National Key Research and Development Program of China (2017YFC1500403) and the National Natural Science Foundation of China (51678299, 52008206).
First author: LIU Kang, male, born in 1995, Postgraduate, majoring in soil dynamics. E-mail: 1948660849@qq.com
Corresponding author: CHEN Guo-xing, male, born in 1963, PhD, Professor, research interests: soil dynamics and geotechnical seismic engineering. E-mail: gxc6307@163.com

continuous rotation of the principal stress axis has a greater impact on the CRR than the jump of the stress axis. Chen et al.[11] carried out a series of undrained dynamic characteristics tests of Nantong silt under complex stress paths, put forward the tangent function relationship between deviatoric strain amplitude and residual excess pore water pressure development for the first time, originally proposed the definition of unit cyclic stress ratio USR, and normalized the liquefaction strength curves under different complex stress paths with USR as an index.

The research upon cyclic undrained characteristics of saturated Calcareous sand is developed recently and the current studies are mainly focusing on the cyclic triaxial testing or simple shear testing. Rasouli et al.[12] found that the strength of liquefaction decreases with initial shear stress ratio for loose Hormuz Calcareous sand whilst increases for dense samples. Liu Hanlong et al.[13] conducted a series of dynamic triaxial tests on MICP cemented calcareous sand. It was found that compared with the samples without cementation treatment, the pore pressure evolution of cemented calcareous sand decelerated, and the CRR and resistance to deformation increased with the improvement of its cementation degree. The test results of Gao ran et al.[14] show that under undrained conditions, the dual normalized pore pressure development characteristics of calcareous sand in the South China Sea conform to the conventional anti sinusoidal function pore pressure model, and the hyperbolic relationship between dynamic deformation modulus and normalized strain is not affected by dry density and particle gradation; A linear relationship between damping ratio and normalized strain under drained condition was introduced. Hyodo et al.[15] and Ma[16] found that the CRR of saturated coral sand is greater than that of terrestrial quartz sand.

Previous studies have shown that the fine particle content FC (mass percentage of soil particles with particle size less than 0.075 mm) has a significant effect on the undrained dynamic characteristics of saturated sand. For example, Polito et al.[17] found that under the fixed relative compactness $D_r$, the CRR of saturated sand remains unchanged in the early stage and subsequently decreases with the increase of FC. This value performs decrease-increase mode with FC under the constant void ratio. The tests of Karim[18] and Wu et al.[19] show that when $D_r$ =30%, the CRR of saturated coarse and fine mixture decreases initially and basically remains unchanged afterwards with the increase of FC, whereas this value decreases and then increases slightly for $D_r$ = 50% or 70%.

In this paper, a series of undrained cyclic loading tests on saturated coral sand of an island and reef in the South China Sea are carried out to simulate the stress path of 90° mutation of principal stress direction angle caused by seismic P-S wave coupling. The influence of cyclic loading direction angle on the deformation and pore pressure development mode of saturated coral sand with different FC and the unified characterization method of liquefaction strength are proposed.

## 2 Methodology

### 2.1 Testing apparatus

GDS hollow cylinder torsional shear apparatus of Nanjing University of technology was used for the test. The static or dynamic loading of axial force $W$, torque $M_T$, internal and external pressures $p_o$ and $p_i$ can be independently controlled simultaneously[20]. The hollow cylindrical sample with the dimensions of $H$ =200 mm, outer diameter $r_o$ =100 mm and inner diameter $r_i$ = 60 mm was prepared. The stress states of hollow cylinder sample and unit body are demonstrated in Fig. 1(a) and Fig. 1(b) respectively. Hight et al.[21] have given the relationship between the loading parameters of hollow cylinder sample ($W$, $M_T$, $p_o$, $p_i$) and the stress parameters of unit body (axial stress $\sigma_z$, radial stress $\sigma_r$, circumferential stress $\sigma_\theta$, shear stress $\tau_{z\theta}$, large principal stress $\sigma_1$, medium principal stress $\sigma_2$, small principal stress $\sigma_3$ and cyclic loading direction angle $\alpha_d$), as shown in Fig. 1(c).

Considering that complicated loading may cause changes in the four components of soil axial strain $\varepsilon_z$, radial strain $\varepsilon_r$, circumferential strain $\varepsilon_\theta$ and shear strain $\gamma_{z\theta}$, the generalized shear strain $\gamma_g$ is introduced to comprehensively characterize the deformation development of soil under complicated loading condition[22–23]

$$\gamma_g = \sqrt{\frac{2\left[\left(\varepsilon_1-\varepsilon_2\right)^2+\left(\varepsilon_1-\varepsilon_3\right)^2+\left(\varepsilon_2-\varepsilon_3\right)^2\right]}{9}} \quad (1)$$

where $\varepsilon_1$, $\varepsilon_2$ and $\varepsilon_3$ are the principal strains corresponding to major, medium and minor principal stresses respectively.

### 2.2 Test material and sample preparation

The experimental material is coral sand on a reef in Spratly Islands. This material is a special marine soil, of which the calcium carbonate content >90% and relative density 2.80[16], formed by the physical, biological and chemical effects of the skeleton of marine organisms. Due to the special formation history, it shows the characteristics of high edge angle, cementation and fragmentation of particles, irregular shape, pores and rough surface[24–25].

The coral sand is firstly dried in a constant temperature

oven at 103 ℃ for 24 hours, and then screened with a standard sieve of 0.075 mm. The particles less than 0.075 mm are defined as fine particles, and the other with size greater than 0.075 mm are used as sand. The fine particles of different mass are mixed with sand to obtain coral sand with different FC, and the grading curves of pure sand, pure fine particles and coral sand with different FC are shown in Fig. 2. The corresponding basic physical indexes are given in Table 1. The maximum and minimum void ratio are measured by ASTM specification[26−27], and the minimum void ratio is measured with a vibration method.

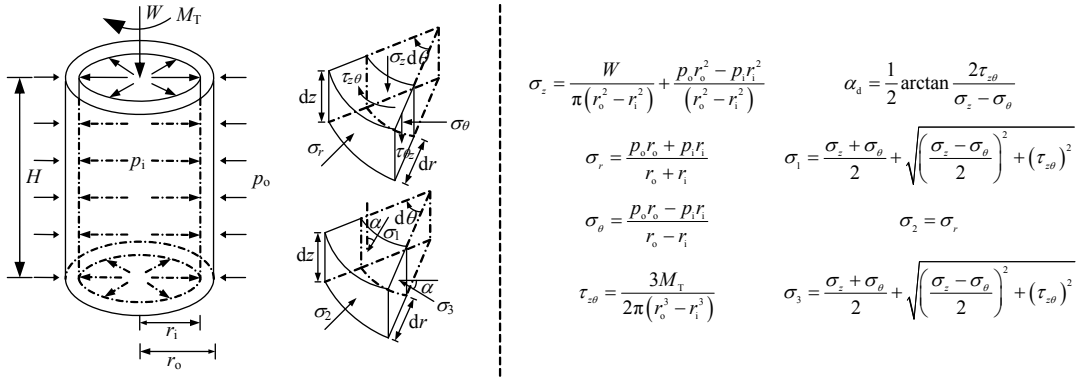


(a) Demonstration of loading on specimen in the hollow cylinder

(b) Stress state of thin element

$$\sigma_z = \frac{W}{\pi\left(r_o^2 - r_i^2\right)} + \frac{p_o r_o^2 - p_i r_i^2}{\left(r_o^2 - r_i^2\right)} \qquad \alpha_d = \frac{1}{2}\arctan\frac{2\tau_{z\theta}}{\sigma_z - \sigma_\theta}$$

$$\sigma_r = \frac{p_o r_o + p_i r_i}{r_o + r_i} \qquad \sigma_1 = \frac{\sigma_z + \sigma_\theta}{2} + \sqrt{\left(\frac{\sigma_z - \sigma_\theta}{2}\right)^2 + \left(\tau_{z\theta}\right)^2}$$

$$\sigma_\theta = \frac{p_o r_o - p_i r_i}{r_o - r_i} \qquad \sigma_2 = \sigma_r$$

$$\tau_{z\theta} = \frac{3M_T}{2\pi\left(r_o^3 - r_i^3\right)} \qquad \sigma_3 = \frac{\sigma_z + \sigma_\theta}{2} - \sqrt{\left(\frac{\sigma_z - \sigma_\theta}{2}\right)^2 + \left(\tau_{z\theta}\right)^2}$$

(c) Calculation of stress state

**Fig. 1 Stress state and stress calculation formulas of hollow cylinder specimen**

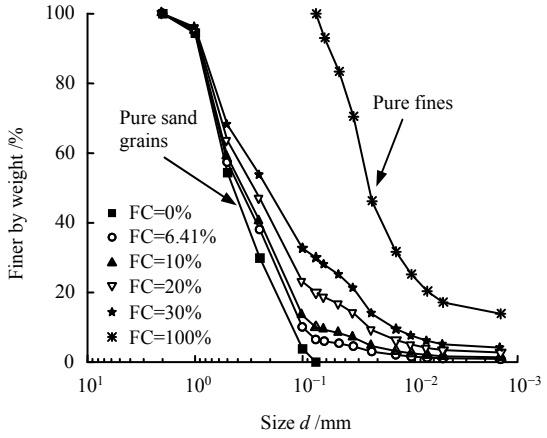


**Fig. 2 Particle size distributions of pure sand, pure fine particles and coral sand with various FCs**

**Table 1 Mechanical properties of pure sand, pure fine particles and coral sand with varying FCs**

| FC /% | $e_{max}$ | $e_{min}$ | $d_{50}$ /mm | $C_u$ | $C_c$ |
|---|---|---|---|---|---|
| 0 | 1.79 | 1.12 | 0.44 | 4.53 | 0.91 |
| 6.41 | 1.72 | 0.99 | 0.38 | 5.41 | 0.71 |
| 10.00 | 1.70 | 0.91 | 0.35 | 6.58 | 0.84 |
| 20.00 | 1.65 | 0.77 | 0.28 | 17.82 | 1.59 |
| 30.00 | 1.62 | 0.69 | 0.21 | 23.69 | 1.19 |
| 100.00 | 1.52 | 0.89 | 0.03 | — | — |

Note: $e_{max}$ and $e_{min}$ are the maximum and the minimum void ratio; $d_{50}$ is the mean particle size; $C_u$ is the uniformity coefficient; and $C_c$ is the coefficient of curvature.

Remolded samples were prepared using dry loading method[28], and the initial target relative compactness is determined $D_r$ =45%. The coral sand is evenly divided into 5 layers and poured into the membrane bearing cylinder of the hollow cylindrical mold. The soil between each layer is scraped[29] to ensure the uniformity of the sample. The sample is saturated with combined measures including $CO_2$ replacement, airless water injection and graded back pressure saturation after the completion of sample loading. When the pore pressure coefficient $B \geqslant 0.97$, the sample is considered to be fully saturated[11]; The saturated specimen shall be uniformly consolidated under the condition of controlling the initial effective mean principal stress $\sigma'_m$ =100 kPa. The coefficient of medium principal stress coefficient is controlled as $b$ = 0.5, and the stress path with the sudden change of the principal stress direction angle by 90° is employed for loading, as shown in Fig. 3.

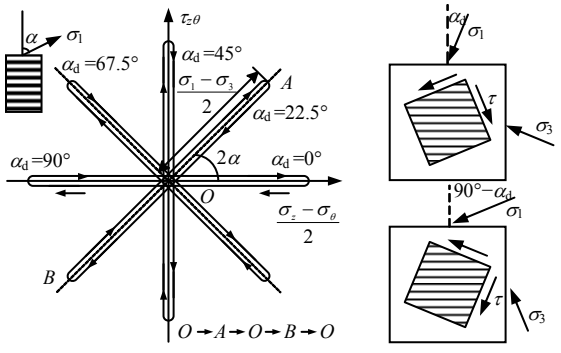


(a) Stress paths

(b) Principal stress direction angle and maximum dynamic shear stress

**Fig. 3 Stress paths of cyclic loadings and the corresponding principal cyclic shear effect plane**

It should be pointed out that for the two different stress paths of cyclic loading direction angle $\alpha_d$ and 90°− $\alpha_d$ , the only difference is that the initial loading direction of the maximum dynamic shear stress acting on the sedimentary surface of the soil element is opposite,

whilst the same effects of other dynamic stresses on the soil element are caused. That shows that the stress effects of the two stress paths of $\alpha_d$ and $90°-\alpha_d$ on the soil element are consistent in essence. The cyclic loading stress paths of $\alpha_d$ and $90°-\alpha_d$ are substantially opposite to each other. The laboratory unit test shows that the difference in the undrained response characteristics of saturated liquefiable soil under the cyclic loading stress paths of[11,28−29] $\alpha_d$ and $90°-\alpha_d$ could be diminished. Therefore, the undrained cyclic loading test of saturated coral sand is carried out at 0°, 22.5° and 45.0° in this study, and the loading frequency is 1 Hz. See Table 2 for the test scheme.

**Table 2 Test scheme**

| ID | FC /% | $\alpha_d$ /(°) | $\sigma'_m$ /kPa | $b$ | CSR | USR | $N_L$/次 |
|---|---|---|---|---|---|---|---|
| 1 | 0 | 0.0 | 100 | 0.5 | 0.25 | 0.188 | Unliquefied |
| 2 | 0 | 22.5 | | | 0.25 | 0.223 | 162 |
| 3 | 0 | 45.0 | | | 0.25 | 0.250 | 78 |
| 4 | 0 | 45.0 | | | 0.32 | 0.320 | 19 |
| 5 | 0 | 0.0 | | | 0.35 | 0.263 | 56 |
| 6 | 6.41 | 0.0 | | | 0.25 | 0.188 | 340 |
| 7 | 6.41 | 22.5 | | | 0.25 | 0.223 | 103 |
| 8 | 6.41 | 45.0 | | | 0.25 | 0.250 | 61 |
| 9 | 6.41 | 0.0 | | | 0.30 | 0.225 | 71 |
| 10 | 6.41 | 0.0 | | | 0.35 | 0.263 | 29 |
| 11 | 10 | 0.0 | | | 0.25 | 0.188 | 72 |
| 12 | 10 | 22.5 | | | 0.25 | 0.223 | 40 |
| 13 | 10 | 45.0 | | | 0.25 | 0.250 | 25 |
| 14 | 10 | 45.0 | | | 0.28 | 0.280 | 17 |
| 15 | 20 | 0.0 | | | 0.25 | 0.188 | 32 |
| 16 | 20 | 22.5 | | | 0.25 | 0.223 | 19 |
| 17 | 20 | 45.0 | | | 0.25 | 0.250 | 14 |
| 18 | 30 | 0.0 | | | 0.25 | 0.188 | 29 |
| 19 | 30 | 22.5 | | | 0.25 | 0.223 | 17 |
| 20 | 30 | 45.0 | | | 0.25 | 0.250 | 8 |

Note: $b$ is the principal stress coefficient; and $N_L$ is the liquefaction vibration number.

The cyclic stress ratio CSR is defined with[23]

$$\mathrm{CSR} = q_{am}/\sigma'_m \quad (2)$$

where $q_{am}$ is the amplitude of deviatoric stress, $q_{am} = (\sigma_1 - \sigma_3)/2 = \sqrt{(\sigma_z - \sigma_\theta)^2/4 + (\tau_{z\theta})^2}$; and $\sigma'_m$ is the initial mean effective stress.

## 3 Results and discussion

Figure 4 shows the undrained response curve of saturated coral sand with FC =20% at $\alpha_d$ = 22.5°. An oblique straight line with a stress path of 45.0° is measured on the ($\tau_{z\theta}$, $(\sigma_z - \sigma_\theta)/2$) stress plane, as shown in Fig. 4(a). This is consistent with the theoretical stress path, and the measured medium principal stress coefficient $b$ is maintained at 0.50 ± 0.015, showing that this test enables accurate simulation of the complex cyclic loading stress path with fixed b value. It can be seen from Fig.4(b) that the excess pore water pressure $u_e$ gradually increases with the cyclic vibration number $N$, whereas different evolution characteristics of loose and saturated quartz sand in land area are found. The $u_e$ of saturated coral sand has no obvious fluctuation at the initial stage of cyclic loading, and the fluctuation increases with $N$ until it reaches $\sigma'_m$. This has good agreement with the test results of Ma et al.[16]. In addition, when $u_e$ is less than 80 kPa, the generalized shear strain $\gamma_g$ increases gradually at low speed. However, the value grows sharply when $u_e$ is greater than 80 kPa, and it exceeds 2.5% when $u_e$ reaches $\sigma'_m$. The test in this study takes $u_e$ reaching $\sigma'_m$ as the initial liquefaction criterion of saturated coral sand.

### 3.1 Pore pressure characteristics of coral sand

The excess pore pressure ratio $R_u$ is defined as the ratio of the peak value of $u_e$ to $\sigma'_m$ in each loading cycle, and the $N$ required for the sample to reach the initial liquefaction state ($R_u$=1.0) is defined as the liquefaction vibration number $N_L$. Fig. 5 shows the relationship between $R_u$ and FC, $N$ of saturated coral sand under different $\alpha_d$ when CSR=0.25. It can be seen that FC and $\alpha_d$ have a significant impact on the development rate of $R_u$. Meanwhile, with the increase of FC, the development rate of $R_u$ increases and $N_L$ decreases, and the manners are followed for with the increase of $\alpha_d$.

Figure 6 presents the relationship between $R_u$ and $N/N_L$ of saturated coral sand. It indicates that FC and $\alpha_d$ have obvious effects on the variation characteristics of $R_u$ with $N/N_L$. Obviously, under the same CSR and FC conditions, $R_u$ at $\alpha_d$ =45° performs fastest evolution with $N/N_L$, and it seems that the classical sinusoidal pore water pressure model proposed by seed et al.[30] is not fully applicable to saturated coral sand. The solid line in Fig. 6 represents the upper and lower boundaries of pore pressure development of calcareous sand in the South China Sea obtained by Gao et al.[14] via a series of dynamic triaxial tests. Apparently, the pore pressure of calcareous sand, when it evolves into the initial liquefaction state, does not reach the effective confining pressure, and that is different from the results of this test. The reason for the deviation may be related to soil properties and test conditions, the latter includes the test instrument and the cyclic loading stress path. The pore pressure evolution of coral sand is within the corresponding envelope given by Gao et al.[14] when $R_u$<0.3. However, when $R_u$> 0.3, the pore pressure the given upper boundary. The shaded part in Fig. 6 is the pore pressure envelope of Monterey quartz sand given by Lee et al.[31], and it is found that the evolved pore pressure of saturated coral sand obviously exceeds the

upper boundary of pore pressure of continental quartz sand.

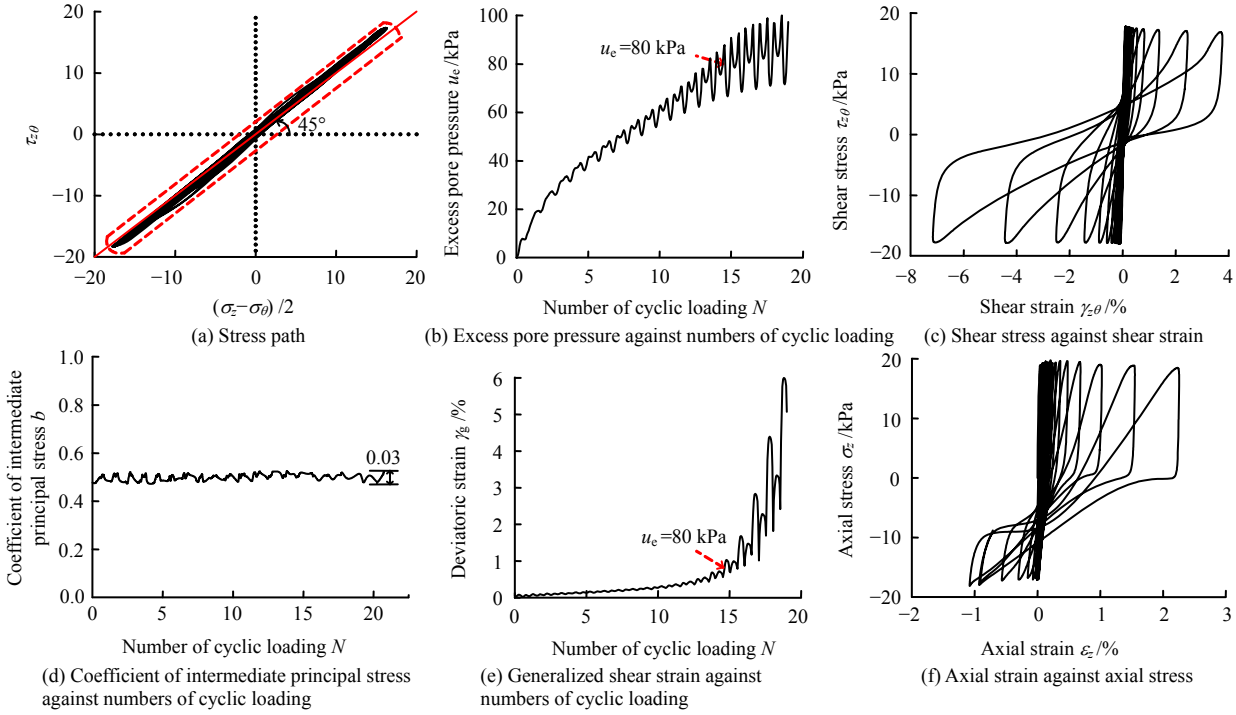


**Fig. 4 Test results of representative data (ID.16)**

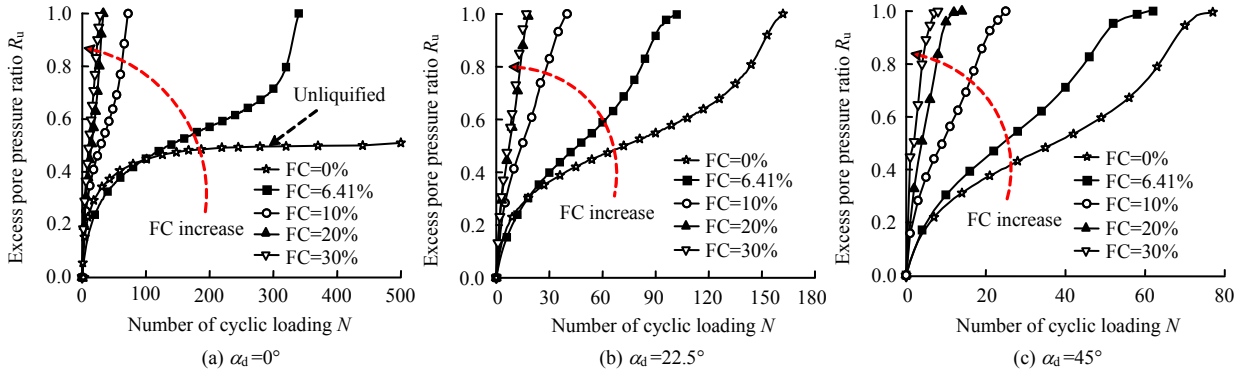


**Fig. 5 Relationship between the excess pore pressure ratio $R_u$ and the number of cycles $N$**

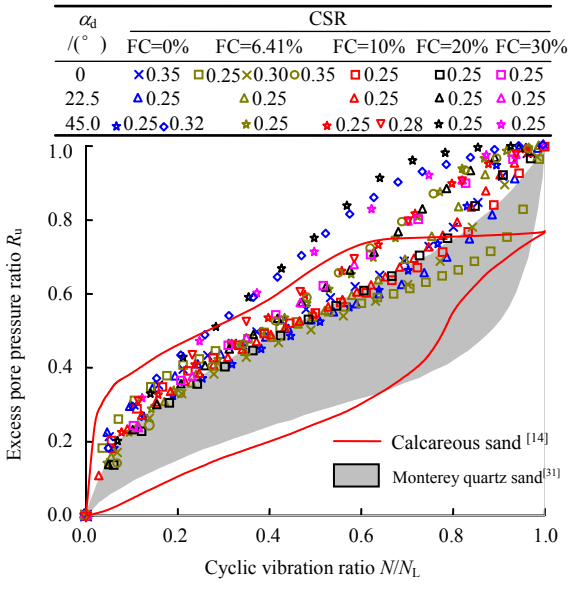


**Fig. 6 Evolution patterns of excess pore water pressure for saturated coral sand with various FCs**

### 3.2 Deformation characterization of calcareous sand

Figure 7 shows the amplitude of normalized generalized shear strain $\gamma_{ga}$ against cycle numbers $N$ for saturated calcareous sand when CSR=0.25. This curve basically follow the same manner for various FC and $\alpha_d$. $\gamma_{ga}$ increases slowly in the early stage of cyclic loading whereas the damage of the saturated calcareous sand is accelerated after $\gamma_{ga}$ reaching 0.5%, and this value dramatically increases with number of cycles subsequently.

Figure 8 shows the evolution of $\gamma_{ga}$ against $R_u$. It can be seen from the figure that under the condition of identical CSR and $\alpha_d$ whilst different FC, the curves of $\gamma_{ga}$ against $R_u$ show similar characteristics. It seems that the CSR and $\alpha_d$ causes little effect on the shape of curves under a fixed FC. The development of $\gamma_{ga}$ performs in a constrained mode for $R_u$<0.4, linearly increasing for 0.4<$R_u$<0.8 and sharply growing for

$R_u > 0.8$.

Chen et al.[11] found that there is a unique relationship between $\gamma_{ga}$ and $R_u$ via the cyclic loading test of silt

$$\gamma_{ga} = a \cdot \tan\left(\frac{\pi}{2} R_u\right) \quad (3)$$

where $a$ is the fitting parameter.

Due to the obvious difference in pore pressure development characteristics between coral sand and terrigenous cohesionless soil, Ma et al.[32] modified Eq. (3) as follows:

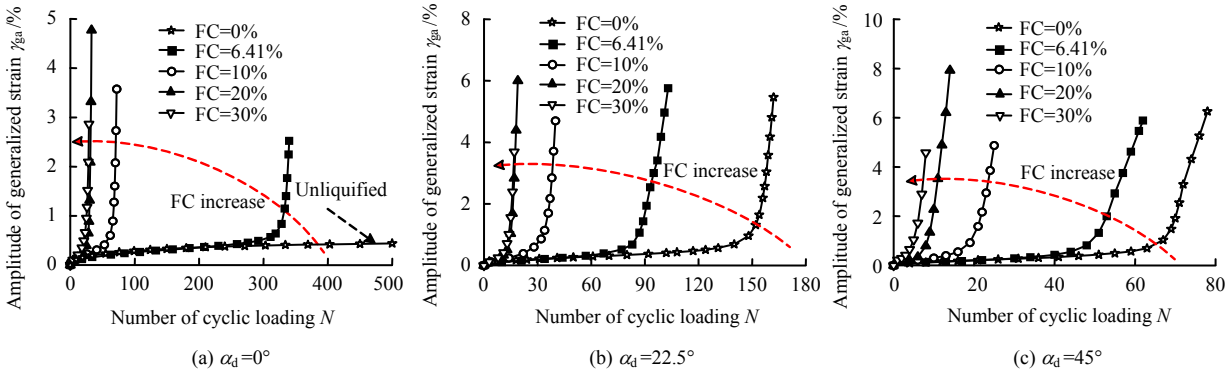


**Fig. 7 Relationships between the generalized shear strain amplitude $\gamma_{ga}$ and the number of cycles $N$**

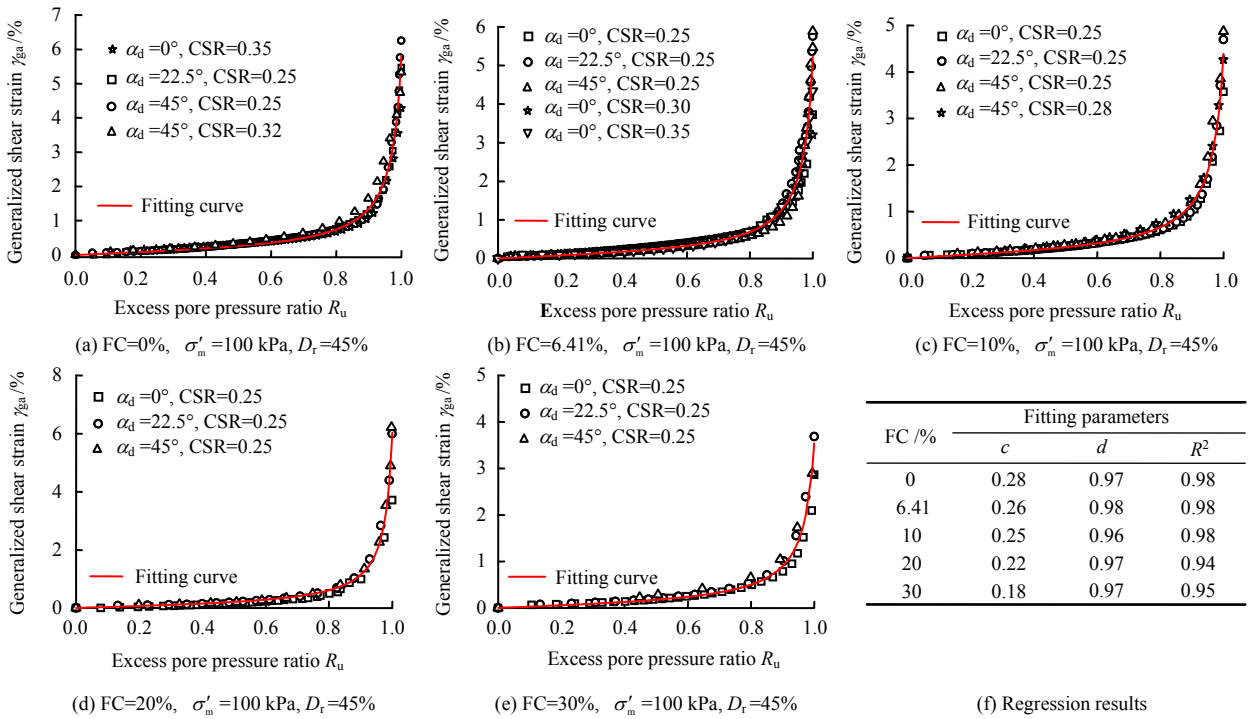


| FC /% | Fitting parameters | | |
|---|---|---|---|
| | $c$ | $d$ | $R^2$ |
| 0 | 0.28 | 0.97 | 0.98 |
| 6.41 | 0.26 | 0.98 | 0.98 |
| 10 | 0.25 | 0.96 | 0.98 |
| 20 | 0.22 | 0.97 | 0.94 |
| 30 | 0.18 | 0.97 | 0.95 |

(f) Regression results

**Fig. 8 Relationships between generalized shear strain and excess pore pressure ratio**

$$\gamma_{ga} = c \cdot \tan\left(\frac{\pi}{2} d R_u\right) \quad (4)$$

where $c$ and $d$ are fitting parameters.

Figure 8 gives good indication that Eq. (4) reaches good agreement with the test data pairs of different FC coral sands and $R_u$, and the correlation coefficient $R^2 > 0.94$. Fig. 9 shows the relationship between fitting parameters $c$, $d$ and FC, where $c$ decreases linearly with the increase of FC. This shows that the parameter $c$ reflects the grading characteristics of coral sand, whilst parameter $d$ is not sensitive to the change of FC ($d \approx 0.97$). Considering Eq. (3) and Eq. (4), $d$ could be deemed as the parameter reflecting soil properties.

### 3.3 Unified evaluation method for liquefaction strength of saturated coral sand

Cyclic loading mode and stress path significantly affects liquefaction strength curve (CSR and $N_L$ curve) of liquefiable soil with CSR as index[9–11]. Chen et al.[11] defined the unit cyclic stress ratio USR as a new index of liquefaction strength, and they pointed out that there is a negative power function relationship between USR and $N_L$, of which

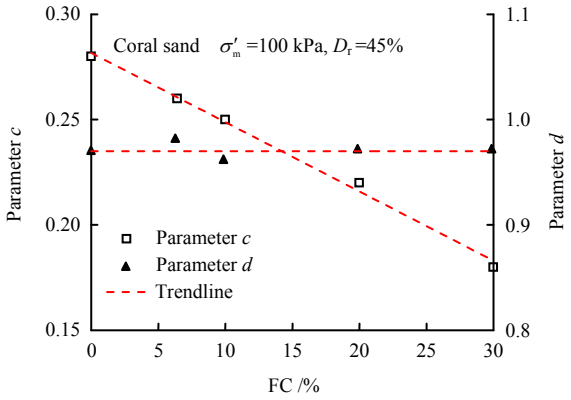


**Fig. 9 Relationships between the fine contents FC and the optimistic fitting parameters *c* and *d***

$$\mathrm{USR}=\alpha_1\alpha_2\cdot\mathrm{CSR} \tag{5}$$

$$\alpha_1=A_{\mathrm{p0}}/A_{\mathrm{M}} \tag{6}$$

$$\alpha_2=\left(1-A_{\mathrm{q0}}/A_{\mathrm{p0}}\right)^{\alpha_3} \tag{7}$$

$$A_{\mathrm{p0}}=\int_0^T\sqrt{\left(\frac{W(t)}{\pi\left(r_{\mathrm{o}}^2-r_{\mathrm{i}}^2\right)}\right)^2\Big/4+\left(\frac{3M_{\mathrm{T}}(t)}{2\pi\left(r_{\mathrm{o}}^3-r_{\mathrm{i}}^3\right)}\right)^2}\,\mathrm{d}t \tag{8}$$

$$A_{\mathrm{q0}}=\left|\int_0^T\left(\sigma_z(t)-p\right)\mathrm{d}t\right|=\left|\int_0^T\left(\frac{W(t)}{\pi\left(r_{\mathrm{o}}^2-r_{\mathrm{i}}^2\right)}\right)\mathrm{d}t\right| \tag{9}$$

where $A_{\mathrm{M}}$ is the reference value $A_{\mathrm{M}}=1.27q_{\mathrm{am}}T$; $T$ is the cycle period; $\alpha_3$ is a parameter reflecting the fuzzy influence of soil properties, taken $\alpha_3=0.1$[11]; $A_{\mathrm{p0}}$ and $A_{\mathrm{q0}}$ are the sum and difference between the magnitude of principal stress caused by external cyclic load and the area enclosed by the time axis in a $T$ when the medium principal stress caused by external cyclic load is 0. Therefore, the essence of USR is to correct CSR by eliminating the difference between the external cyclic load and the area enclosed by the time axis under different loading modes. Compared with CSR, USR can normalize the liquefaction strength curves of sand under different complex cyclic loading stress paths. It should be noted that for conventional cyclic triaxial test or cyclic torsional shear test, USR degenerates into CSR when $\alpha_1=\alpha_2=1$.

Figure 10 shows the relationship between USR and $N_{\mathrm{L}}$ of saturated coral sand. It can be found that when FC is a fixed value, $N_{\mathrm{L}}$ increases with the decrease of USR, represented with a negative power function relationship between each other. This is consistent with the test results of Ma et al.[28], which further proves the applicability of USR as the liquefaction strength index of soil element under different cyclic loading modes and stress paths. In addition, with the increase of FC, the USR−$N_{\mathrm{L}}$ curve offsets downward, which shows that the increase of fine particle content will significantly reduce the liquefaction strength of saturated coral sand. This is reasonable as under fixed relative density $D_{\mathrm{r}}$ condition, the number of sand particles constituting the soil skeleton decreases with the increase of FC, and is replaced by some fine particles participating in the composition, which will consequently reduce the contact area between the particles constituting the force chain transmission. In addition, the other part of the fine particles is only filled in the pores of the soil skeleton and do not play the role of the force chain. The combined action causes the liquefaction strength of saturated coral sand to decrease with the increase of FC.

For sand with different FCs, there must be a threshold fine grain content $\mathrm{FC_{th}}$ to classify sandy soil and quasi fine grain soil. Rahman et al.[33] proposed a semi empirical formula for predicting $\mathrm{FC_{th}}$

$$\mathrm{FC_{th}}=0.40\left(\frac{1}{1+\exp\left(0.5-0.13\chi\right)}+\frac{1}{\chi}\right) \tag{10}$$

where $\chi=d_{10}^{\mathrm{s}}/d_{50}^{\mathrm{f}}$ is the particle size ratio; $d_{10}^{\mathrm{s}}$ is the average particle size of pure sand; $d_{50}^{\mathrm{f}}$ is the average particle size of pure fine particles. The coral sand $\mathrm{FC_{th}}$ used in this test is 0.30, and the coral sands with different FCs are subject to sandy soil.

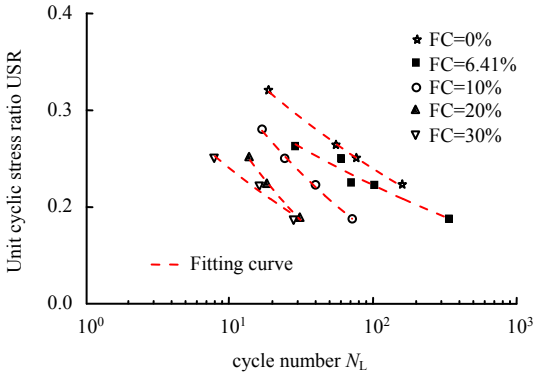


**Fig. 10 Relationship between USR and cycle number $N_{\mathrm{L}}$ required to trigger liquefaction**

Thevanayagam et al.[34] proposed the concept of equivalent skeleton void ratio $e_{\mathrm{sk}}^*$ to describe the influence of the degree of fine particles participating in the composition of soil skeleton on the contact state of sand particles with different FCs. It is defined as the ratio of sand skeleton particle volume to pore volume between each other:

$$e_{\mathrm{sk}}^{*}=\frac{e+(1-b)\mathrm{FC}}{1-(1-b)\mathrm{FC}} \tag{11}$$

where $b$ is fine particle influence coefficient, $0\leqslant b\leqslant 1$. Compared with the void ratio $e$, $e_{\mathrm{sk}}^{*}$ can comprehensively reflect the effects of fine particle content, physical state and contact state between particles on the physical properties of sand.

Mohammadi et al.[35] gave a simplified formula for predicting $b$ value as follows:

$$b=\left\{1-\exp\left[-\frac{0.3}{k}\right]\right\}\left(r\cdot\frac{\mathrm{FC}}{\mathrm{FC}_{\mathrm{th}}}\right)^{r} \tag{12}$$

where $k=1-r^{0.25}$, $r=\chi^{-1}$.

In engineering practice, the CSR required for the sample to meet the specified liquefaction standard when $N_{\mathrm{L}}$=15 is usually used as the liquefaction strength of soil, and hence the unit liquefaction strength $\mathrm{USR}_{15}$ of soil can be defined as the USR required for the sample for meeting the requirement. Fig.11 shows the relationship between saturated coral sand $\mathrm{USR}_{15}$ and $e_{\mathrm{sk}}^{*}$ under different FC conditions. It is found that $\mathrm{USR}_{15}$ decreases with the increase of $e_{\mathrm{sk}}^{*}$, indicating a good negative power function relationship between each other

$$\mathrm{USR}_{15}=A\cdot e_{\mathrm{sk}}^{*\,-m} \tag{13}$$

where $A$ and $m$ are fitting parameters, and the correlation coefficient derived for Eq. 13 is $R^2$ =0.91.

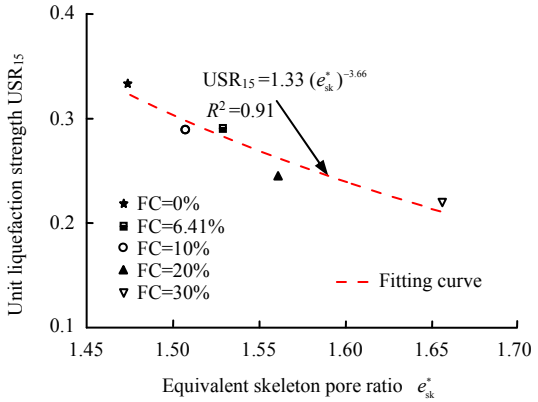


**Fig. 11 Relationship between $\mathrm{USR}_{15}$ and the equivalent skeleton pore ratio $e_{\mathrm{sk}}^{*}$**

Figure 12 illustrates the relationship curves between $\mathrm{USR}_{15}$ and the test data upon five types of sand in the literatures. The unique relation between $\mathrm{USR}_{15}$ and $e_{\mathrm{sk}}^{*}$ has been found for these five types of sands. Meanwhile, the liquefaction strength of coral sand is obviously greater than that of these five types of continental quartz sand. The reason for this is that the coral sand has the characteristics of high edge angle, brittleness, irregular shape, internal pores, cementation, and the particles are sub angular−flakes, which leads to the large occluding effect among particles, slow growth of pore pressure and difficult reorganization of particle arrangement during cyclic loading, and consequently it is not easy to be liquefied.

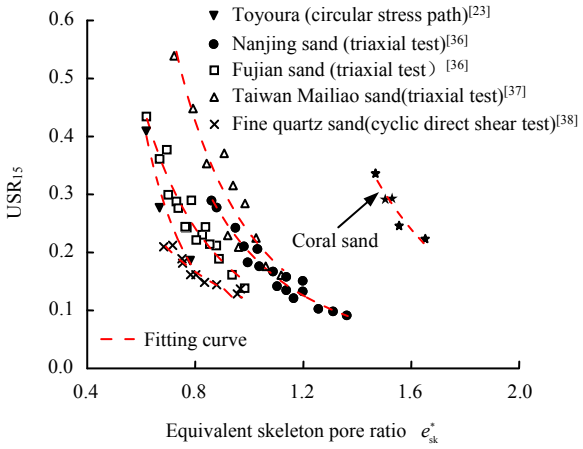


**Fig. 12 Relationship between $\mathrm{USR}_{15}$ and equivalent skeleton pore ratio $e_{\mathrm{sk}}^{*}$ for five types of sand**

In conclusion, $e_{\mathrm{sk}}^{*}$ can comprehensively reflect the impact of the physical characteristics of saturated coral sand on $\mathrm{USR}_{15}$, and therefore is considered a suitable physical characteristic index to describe $\mathrm{USR}_{15}$. Further verification is required for the university of $e_{\mathrm{sk}}^{*}$ in reflection of $\mathrm{USR}_{15}$ via various liquefaction test data of saturated sand under different cyclic loading modes and stress paths.

## 4 Conclusion

(1) The development of excess pore pressure of saturated coral sand obviously exceeds the upper boundary of that of continental quartz sand, and the former performs higher rate of evolution.

(2) The deformation pattern of the saturated calcareous sand behaves the manner of ‘gentle−sharp’. A constitutive model based on the generalized shear strain $\gamma_{\mathrm{ga}}$ and FC has been developed for the excessive pore water pressure of the calcareous sand.

(3) The unit cyclic stress ratio USR is introduced to quantitatively characterize the complex cyclic stress level. Based on the binary medium theory, the unified expression of liquefaction strength of saturated coral sand is established, and the applicability of this method is verified by the test data of five kinds of sandy soils in the literature.

## References

[1] MEJIA L H, YEUNG M R. Liquefaction of coralline soils during the 1993 guam earthquake[C]//Earthquake-induced Movements and Seismic Remediation of Existing Foundations and Abutments: Proceedings of Sessions Held in Conjunction with the ASCE Convention in San Diego. San Diego: [s. n.], 1995: 33−48.

[2] CHOCK G, KINDRED T, ROBERTSON I, et al. Compilation of observations of the October 15, 2006 Kiholo bay (Mw 6.7) and Mahukona (Mw 6.0) Earthquakes, Hawai'i[R]. [S. l.]: Earthquake Engineering Research Institute (EERT), 2006.

[3] OLSON S M, GREEN R A, LASLEY S, et al. Documenting liquefaction and lateral spreading triggered by the 12 January 2010 haiti earthquake[J]. Earthquake Spectra, 2012, 27(Suppl. 1): S93−S116.

[4] China Earthquake Networks Center. Distribution map of earthquake epicenters in China and neighboring areas (1∶5 million)[M]. Beijing: Seismological Press, 2015.

[5] GUO Ying, LUAN Mao-tian, HE Yang, et al. Effect of variation of principal stress orientation during cyclic loading on undrained dynamic behavior of saturated loose sands[J]. Chinese Journal of Geotechnical Engineering, 2005, 27(4): 403−409.

[6] LI Jian-guo. Experimental research on dynamic behavior of saturated calcareous sand under wave loading[D]. Wuhan: Institute of Rock and Soil Mechanics, Chinese Academy of Sciences, 2005.

[7] YU Hai-zhen. Experimental study on dynamic characteristics of saturated calcareous sand under complex stress conditions[D]. Wuhan: Huazhong University of Science and Technology, 2006.

[8] XU Cheng-shun, GAO Ying, DU Xiu-li, et al. Dynamic strength of saturated sand under bi-directional cyclic loading[J]. Chinese Journal of Geotechnical Engineering, 2014, 36(12): 2335−2340.

[9] HUANG B, CHEN X, ZHAO Y. A new index for evaluating liquefaction resistance of soil under combined cyclic shear stresses[J]. Engineering Geology, 2015, 199: 125−139.

[10] SIVATHAYALAN S, LOGESWARAN P, MANMATHARAJAN V. Cyclic resistance of a loose sand subjected to rotation of principal stresses[J]. Journal of Geotechnical and Geoenvironmental Engineering, 2015, 141(3): 04014113.

[11] CHEN G X, WU Q, ZHOU Z L, et al. Undrained anisotropy and cyclic resistance of saturated silt subjected to various patterns of principal stress rotation[J]. Géotechnique, 2019(1): 1−47.

[12] RASOULI M R, MORADI M, GHALANDARZADEH A. Effects of initial static shear stress orientation on cyclic behavior of calcareous sand[J]. Marine Georesources and Geotechnology, 2021, 39(5): 554−568.

[13] LIU Han-long, XIAO Peng, XIAO Yang, et al. Dynamic behaviors of MICP-treated calcareous sand in cyclic tests[J]. Chinese Journal of Geotechnical Engineering, 2018, 40(1): 38−45.

[14] GAO Ran, YE Jian-hong. Experimental investigation on the dynamic characteristics of calcareous sand from the reclaimed coral reef islands in the South China Sea[J]. Rock and Soil Mechanics, 2019, 40(10): 1−13.

[15] HYODO M, HYDE A F L, ARAMAKI N. Liquefaction of crushable soils[J]. Géotechnique, 1998, 48(4): 527−543.

[16] MA Wei-jia, CHEN Guo-xing, LI Lei, et al. Experimental study on liquefaction characteristics of saturated coral sand in Nansha Islands under cyclic loading[J]. Chinese Journal of Geotechnical Engineering, 2019, 41(5): 981−988.

[17] POLITO C P, MARITIN II J R. Effects of Nonplastic Fines on the Liquefaction Resistance of Sands[J]. Journal of Geotechnical & Geoenvironmental Engineering, 2001, 127(5): 408−415.

[18] KARIM M E, ALAM M J. Effect of non-plastic silt content on the liquefaction behavior of sand–silt mixture[J]. Soil Dynamics & Earthquake Engineering, 2014, 65: 142−150.

[19] WU Qi, CHEN Guo-xing, ZHOU Zheng-long, et al. Experimental investigation on liquefaction resistance of fine-coarse-grained soil mixtures based on the theory of intergrain contact state[J]. Chinese Journal of Geotechnical Engineering, 2018, 40(3): 475−485.

[20] ZHOU Zheng-long, CHEN Guo-xing, WU Qi. Analysis of capabilities of stress paths of HCA to simulate principal stress rotation under four-direction dynamic loads[J]. Rock and Soil Mechanics, 2016, 37(Suppl. 1): 126−132.

[21] HIGHT D W, GENS A, SYMES M J. The development of a new hollow cylinder apparatus for investigating the effects of principal stress rotation in soils[J]. Géotechnique, 1983, 33(4): 355−383.

[22] YANG Z X, LI X S, YANG J. Undrained anisotropy and rotational shear in granular soil[J]. Géotechnique, 2007, 57(4): 371−384.

[23] ISHIHARA K, YAMAZAKI A. Analysis of wave-induced liquefaction in seabed deposits of sand[J]. Soils and Foundations, 1984, 24(3): 85−100.

[24] LIU Cong-quan, WANG Ren. Preliminary research on physical and mechanical properties of calcareous sand[J]. Rock and Soil Mechanics, 1998, 19(3): 32−37.

[25] WANG Ren, SONG Chao-jing, ZHAO Huan-ting, et al. The coral reef engineering geology of the spratly islands[M]. Beijing: Science Press, 1997.

[26] ASTM. D4254-14 Standard test methods for minimum index density and unit weight of soils and calculation of relative density[S]. [S. l.]: [s. n.], 2006.

[27] ASTM. D4253-14 Standard test methods for maximum index density and unit weight of soils using a vibratory table[S]. [S. l.]: [s. n.], 2006.

[28] MA Wei-jia, CHEN Guo-xing, WU Qi. Experimental study on liquefaction resistance of coral sand under complex loading conditions[J]. Rock and Soil Mechanics, 2020, 41(2): 535−542, 551.

[29] ZHOU Zheng-long, CHEN Guo-xing, ZHAO Kai, et al. Effect of the direction angle of cyclic loading on undrained cyclic behavior of saturated silt[J]. Rock and Soil Mechanics, 2018(1): 36−44.

[30] SEED H B, LYSMER J, MARTIN P P. Pore-water pressure changes during soil liquefaction[J]. Journal of the Geotechnical Engineering, 1976, 102(4): 323−346.

[31] LEE K L, ALBAISA A. Earthquake induced settlements in saturated sands[J]. Journal of the Geotechnical engineering Division, 1974, 100(4): 387−406.

[32] MA Wei-jia, CHEN Guo-xing, QIN You, et al. Experimental studies on effects of initial major stress direction angles on liquefaction characteristics of saturated coral sand[J]. Chinese Journal of Geotechnical Engineering, 2020, 42(3): 592−600.

[33] RAHMAN M M, LO S R, GNANENDRAN C T. On equivalent granular void ratio and steady state behaviour of loose sand with fines[J]. Canadian Geotechnical Journal, 2008, 45(10): 1439−1456.

[34] THEVANAYAGAM S, SHENTHAN T, MOHAN S, et al. Undrained fragility of clean sands, silty sands, and sandy silts[J]. Journal of the Geotechnical and Geoenvironmental Engineering, 2002, 128(10): 849−859.

[35] MOHAMMADI A, QADIMI A. A simple critical state approach to predicting the cyclic and monotonic response of sands with different fines contents using the equivalent intergranular void ratio[J]. Acta Geotechnica, 2015, 10(5): 587−606.

[36] WU Qi, CHEN Guo-xing, ZHU Yu-meng, et al. Evaluating liquefaction resistance of saturated sandy soils based on equivalent skeleton void ratio[J]. Chinese Journal of Geotechnical Engineering, 2018, 40(10): 1912−1922.

[37] HUANG Y T, HUANG A B, KUO Y C, et al. A laboratory study on the undrained strength of a silty sand from Central Western Taiwan[J]. Soil Dynamics and Earthquake Engineering, 2004, 24(9): 733−743.

[38] CHANG W J, HONG M L. Effects of clay content on liquefaction characteristics of gap-graded clayey sands[J]. Soils and Foundations, 2008, 48(1): 101−114.